Chinese J. Chem. Eng., **10** (4) 416 – 419 (2002)

Bubble Formation Characteristics from a Sieve Tray with Liquid Cross-flow

XU Songlin(许松林)* and XU Shimin(徐世民)
National Engineering Research Center for Distillation Technology, Tianjin University, Tianjin 300072, China

Abstract An apparatus, designed to simulate bubbling of a sieve tray operated in froth regime, was employed. Bubble contact angles in and above the incipient weeping regime for an air-water-plexiglas system were investigated. The influence of both liquid cross-flow and gas up-flow upon bubble contact angles was examined. A model considering the influence of liquid cross-flow was developed to predict bubble size from a sieve hole in froth operation regime. The comparison shows that the bubble sizes predicted by the present model are consistent with our experimental values and the available published experimental data.
Keywords bubble size, sieve tray, contact angle

1 INTRODUCTION

A sieve tray could be operated in different regimes, which include bubble, emulsion, froth and spray regimes, *etc.* There are a lot of evidences that the tray efficiency is different in different regimes. Bubble formation is the basic characteristic of all operation regimes[1,2]. Bubble size, gas phase hold-up, and relative velocity between phases are important hydrodynamic parameters determining interfacial area and mass transfer coefficient, which are needed for plate design and scale-up. Many studies of bubbling from single holes have been reported to elucidate the mechanism of bubbling on multi-hole sieve trays[3–6]. For the most part, the results have been disappointing. The models have been developed only for fairly simple ideal cases, in which bubbling is at low gas rates and liquid is static, and have not yet been extended satisfactorily to multi-hole trays with liquid cross-flow. The main aims of this study are:

(1) To ascertain the influence of liquid cross-flow and gas up-flow velocities on contact angles of a bubble formed from an orifice on a sieve tray;

(2) To develop a model for predicting the bubble size formed from a sieve tray in practical operation regime.

2 EXPERIMENTAL APPARATUS AND PROCEDURE

The experimental apparatus, shown schematically in Fig. 1, comprised of three main components: a plexiglas simulation column, a high speed camera and a light source. Experiments were carried out in the plexiglas simulation column using air/water system. The sieve tray was made up of a 15.0×6.0×0.5 cm rectangular plexiglas plate with eight 3 mm diameter sieve holes. All orifice surfaces were ground smooth and the edges were carefully machined to have a sharp 90 degrees profile. In order to keep a certain thickness of liquid holdup, a height-adjustable outlet weir of 15, 25, 38, 50 mm was mounted respectively. After passing through a calibrated rotameter and a down-comer, water flowed across the plate smoothly. Meanwhile, the air was supplied from a compressed gas cylinder and ran through sieve holes after being mixed in a chamber.

By using the photographic method, the bubble formation characteristics and the effect of gas up-flow velocity on bubble frontal and rear angles for both stagnant and flowing liquid conditions were investigated. For each experimental run, three sample pictures were taken and the following contact angles reported are the average of the three values.

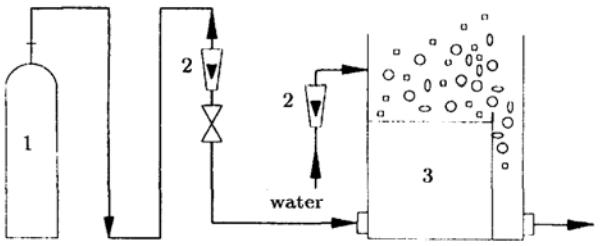

Figure 1 Schematic diagram of apparatus
1—compressed air cylinder; 2—rotameter;
3—simulation column

3 EXPERIMENTAL RESULTS AND DISCUSSION

3.1 Relationship between gas up-flow velocities and contact angles

The frontal and rear contact angles (shown in Fig. 2) measured were reproducible to within 3 degrees and the gas up-flow velocity was the averaged value of

Received 2001-03-06, accepted 2001-11-01.
* To whom correspondence should be addressed.

three measurements. The effect of gas up-flow velocity on bubble frontal and rear contact angles is shown in Fig. 3.

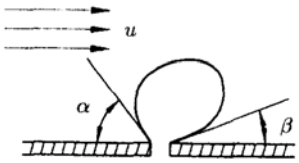

Figure 2 Side view of a bubble

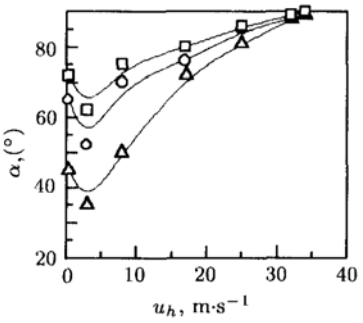

(a)

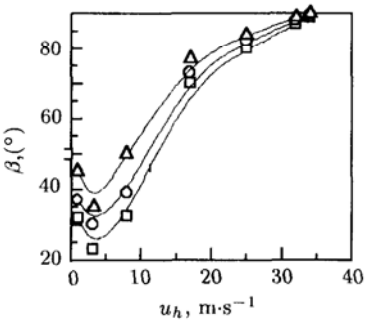

(b)

Figure 3 Effect of gas up-flow velocity on frontal and rear contact angles

U, cm·s^{-1}: —△— 0; —○— 1.85; —□— 6.17

For each liquid cross-flow velocity considered, the frontal and rear contact angles decreased initially with increasing gas hole velocity to a minimum value before increased at higher velocities. The lowest point in each curve corresponded to the stage at which incipient weeping occurred and bubble resided for the longest time. Bubble contact angles (both frontal and rear contact angles) were larger at higher gas up-flow velocities than those at the incipient weeping point since shorter residence time led to smaller bubbles. At gas flow rates lower than that for incipient weeping, weeping persisted for several seconds until the gas chamber pressure exceeded that at the orifice, then bubbles were emitted at a high speed for a short period before weeping started again. Because of this activity, the residence time for each bubble was short so that the bubble contact angles were still larger than those for incipient weeping. The experiments demonstrated that the bubbles exhibited a minimum contact angle for both stagnant and flowing liquids and both frontal and rear angles were strongly influenced by the liquid cross-flow velocity and gas up-flow velocity. With a further increase of gas up-flow velocity, bubbles jetted through sieve holes continually and formed a gas column, and both frontal and rear contact angles were nearly 90°. At different experimental liquid cross-flow rates, the gas up-flow velocities leading to gas column were nearly the same. The main reason was that the effects of different clear liquid heights at varied experimental liquid cross-flow rates were less significant compared with those of large gas up-flow velocities on the formation of gas column.

3.2 Predication of bubble sizes from sieve tray in froth regime

When a sieve tray operated in froth regime, there is a froth layer on the plate. Under this condition, the fluid across the tray is affected not only by the force from horizontal liquid flow but also by the force from gas up-flow passing through the liquid vertically. Then the bubbles in the froth layer bear forces in both vertical and horizontal directions. In the following, a detail analysis is given to describe how a bubble forms under the influence of the two forces.

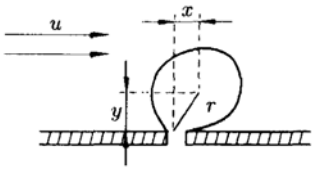

Figure 4 A model for bubble formation from a sieve hole with liquid cross-flow

Within the time t for a bubble detachment, the distances for a bubble to travel in the x and y directions are shown in Fig. 4, where the bubble radius r achieved in time t is given by

$$r^2 = x^2 + y^2 \tag{1}$$

The size of bubble formed within time t is defined as follows

$$Gt = \frac{4}{3}\pi r^3 \tag{2}$$

and

$$G = \frac{\pi}{4} d_0^2 u_h \tag{3}$$

where d_0 is the diameter of sieve hole (m) and u_h is the velocity of gas through the hole(m·s^{-1}).

Basic equations for the bubble motion in the vertical and horizontal directions are:

horizontal direction

$$\frac{d}{dt}\left(\frac{2}{3}\pi\rho r^3 u\right) = n\pi\mu r(U-u) \tag{4}$$

vertical direction

$$\frac{\mathrm{d}}{\mathrm{d}t}\left(\frac{2}{3}\pi\rho r^3 v\right)=\frac{4}{3}\pi\Delta\rho g r^3-n\pi\mu r v \tag{5}$$

The bubble motions in horizontal and vertical directions are analyzed in the following parts respectively.

3.2.1 *Motion in horizontal direction*

Derived from Eq. (2)

$$\frac{\mathrm{d}r}{\mathrm{d}t}=\frac{G}{4\pi}\frac{1}{r^2} \tag{6}$$

Substituting Eq. (6) into Eq. (4) for horizontal motion of the bubble, we get

$$\frac{\mathrm{d}u}{\mathrm{d}r}+3u\left(\frac{1}{r}+\frac{6\pi n\gamma}{G}\right)=\frac{6\pi n\gamma U}{G} \tag{7}$$

let $C=\dfrac{6\pi n\gamma}{G}$, then

$$\frac{\mathrm{d}}{\mathrm{d}r}[ur^3\exp(Cr)]=UCr^3\exp(Cr) \tag{8}$$

By integrating Eq. (8), we have

$$u=\frac{G^2U}{36\pi^2n^2\gamma^2r^2}\cdot\left\{(Cr)^2-3Cr+6-\frac{6}{Cr}[1-\exp(Cr)]\right\} \tag{9}$$

since

$$u=\frac{\mathrm{d}x}{\mathrm{d}t}=\frac{G}{4\pi r^2}\frac{\mathrm{d}x}{\mathrm{d}r}$$

we have

$$\frac{\mathrm{d}x}{\mathrm{d}r}=\frac{GU}{9\pi n^2\gamma^2}\cdot\left\{(Cr)^2-3Cr+6-\frac{6}{Cr}[1-\exp(Cr)]\right\} \tag{10}$$

Integrating Eq. (10) yields

$$x=\frac{GU}{9\pi n^2\gamma^2C}\left[\frac{1}{3}(Cr)^3-\frac{3}{2}(Cr)^2+6Cr-6E(Cr)\right] \tag{11}$$

in which

$$E(Cr)=\int_0^{Cr}\frac{1-\mathrm{e}^{-Cr}}{Cr}\mathrm{d}(Cr)=Cr-\frac{(Cr)^2}{2\times 2!}+\frac{(Cr)^3}{3\times 3!}-\frac{(Cr)^4}{4\times 4!}+\cdots\cdots$$

Eq. (11) describes the motion of a bubble in horizontal direction.

3.2.2 *Motion in vertical direction*

By a treatment analogous to that for horizontal motion, eliminating the t term, we get

$$\frac{\mathrm{d}v}{\mathrm{d}t}+3v\left[\frac{1}{r}+\frac{2\pi n\gamma}{G}\right]=\frac{8\pi gr}{G} \tag{12}$$

By using the same method as above

$$v=\frac{8\pi g}{G}\frac{1}{C^3}\left[(Cr)^2-5Cr+20-\frac{60}{Cr}+\frac{120}{(Cr)^2}-\frac{120}{(Cr)^3}\right] \tag{13}$$

since

$$v=\frac{\mathrm{d}y}{\mathrm{d}t}=\frac{G}{4\pi r^2}\frac{\mathrm{d}y}{\mathrm{d}r}$$

we have

$$\frac{\mathrm{d}y}{\mathrm{d}r}=\frac{8}{9}\frac{g}{n^2\gamma^2C^3}\left\{(Cr)^4-5(Cr)^3+20(Cr)^2-60Cr+120-\frac{120}{Cr}[1-\exp(-Cr)]\right\} \tag{14}$$

Integrating Eq. (14) yields

$$y=\frac{8}{9}\frac{g}{n^2\gamma^2C^4}\left[\frac{1}{5}(Cr)^5-\frac{5}{4}(Cr)^4+\frac{20}{3}(Cr)^2+30(Cr)^2+120Cr-120E(Cr)\right] \tag{15}$$

This is the equation describing the motion of a bubble in vertical direction.

3.2.3 *Prediction of bubble size*

Substituting Eqs. (11) and (15) into Eq. (1), after simplifying and omitting the insignificant elements, and using the parameter $n=6$, which is suitable for air/water system in Stokes law for drag force, we obtain

$$1.95\times 10^8 r^{10}+2.08U^2r^6=d_0^8u_h^4 \tag{16}$$

In the presence of horizontal liquid flow, the bubble size can be calculated from Eq. (16), in which Newton-Cotes method is valid.

To evaluate the precision of the present model for predicting bubble size from a sieve hole with liquid cross-flow, photographic method was applied to obtain the bubble size distribution in a single sieve hole. Table 1 shows the comparison between the bubble sizes of our experimental values and the computed values.

Table 1 Comparison between experimental and calculated bubble sizes

$u_h=7.2\,\mathrm{cm\cdot s^{-1}}$			$u_h=9.3\,\mathrm{cm\cdot s^{-1}}$			$u_h=10.0\,\mathrm{cm\cdot s^{-1}}$		
Δh, cm	d_b, cm	d_c, cm	Δh, cm	d_b, cm	d_c, cm	Δh, cm	d_b, cm	d_c, cm
1.5	1.1	1.09	2.4	1.25	1.21	2.8	1.7	1.24

From Table 1, it is obvious that there is a good agreement between the bubble sizes of our experimental values and the calculated values.

Rapper *et al.*[7] conducted experiments on measuring bubble sizes from a sieve tray with a wide range of gas up-flow velocities and different sieve holes (d_0 is 1.6, 6.4, 12.7, 19.1 mm, respectively). Under the same conditions, calculated values by the present model were also compared with the experimental values given by Rapper *et al.*[7] (the shadow part shown in Fig. 5).

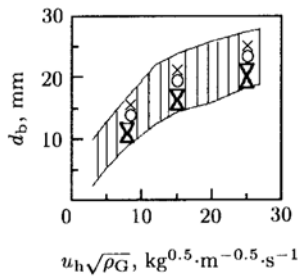

Figure 5 Comparison between predicted values and the experimental data in literature
d_h, mm: △ 1.6; ▽ 6.4; ○ 12.7; × 19.1

From Fig. 5, we see that all predicted bubble diameters fall within the range of experimental values[7].

4 CONCLUSIONS

A simulation column was used to investigate bubbling characteristics from a sieve hole with liquid cross-flow. The measurements of the frontal and rear contact angles for a bubble show that the minimum values correspond to the stage at which incipient weeping occurs and the bubbles reside for the longest time. With a further increase of gas up-flow velocity, bubbles jet from the sieve hole continually and form a gas column. A theoretical model for predicting bubble formation from a sieve hole is developed. Bubble sizes predicted by the model show a good correspondence with our experimental values and literature data.

NOMENCLATURE

C	parameter
d_b	bubble diameter, m
d_c	calculated bubble size, m
d_0	sieve hole diameter, m
G	gas flow-rate, m^3·s^{-1}
g	acceleration of gravity, m·s^{-2}
Δh	vertical distance of bubble center to sieve tray, m
n	constant(=6) in Stokes's fluid drag equation $F = n\pi\mu ur$
r	bubble radius, m
t	time, s
U	horizontal velocity of liquid flow, m·s^{-1}
u	horizontal velocity of bubble center, m·s^{-1}
u_h	gas hole velocity, m·s^{-1}
v	vertical velocity of bubble center, m·s^{-1}
x	horizontal co-ordinate of bubble center to orifice, m
y	vertical co-ordinate of bubble center to orifice, m
α	bubble frontal contact angle, (°)
β	bubble rear contact angle, (°)
μ	absolute liquid viscosity, Pa·s
γ	kinematic liquid viscosity, m^2·s^{-1}
ρ	liquid phase density, kg·m^{-3}
ρ_G	gas phase density, kg·m^{-3}
$\Delta\rho$	difference between liquid and gas density, kg·m^{-3}

REFERENCES

1 Zuiderweg, F.J., "Distillation composition profiles-what do they tell us?", *Trans IChemE*, **77** (A6), 475—481 (1999).
2 Lockett, M.J., Distillation Tray Fundamentals, Cambridge University Press, Cambrige, 37—54(1989).
3 Antoniadis, D., Mantzavinos, D., Stamatoudis, M., "Effect of chamber volume and diameter on bubble formation at plate orifices", *Trans IChemE*, **70** (A1), 161—165 (1992).
4 Barnea, D., Shemer, L., "Rise velocity of large bubbles in stagnant liquid in a non-circular duct", *Int. J. Multiphase Flow*, **12** (5), 1025—1027 (1986).
5 Darton, R.C., Sun, K.H., "The effect of surfactant on foam and froth properties", *Trans IChemE*, **77** (A6), 535—542 (1999).
6 Leibson, I., Holcomb, E.G., Cacoso, G., "Rate of flow and mechanics of bubble formation from single submerged orifices", *AIChE J*, **2** (2), 296—304 (1956).
7 Rapper, J.A., Kearney, M.S., Burgess, J.M., Fell, C.J.D., "The structure of industrial sieve tray froths", *Chem Eng Sci*, **37** (4), 501—506 (1982).